Journal of Thermal Analysis and Calorimetry
https://doi.org/10.1007/s10973-020-10292-y

Free convective heat transfer of a non-Newtonian fluid in a cavity containing a thin flexible heater plate: an Eulerian–Lagrangian approach

Mohammad Ghalambaz[1,2] · S. A. M. Mehryan[3] · Reza Kalantar Feeoj[4] · Ahmad Hajjar[5] · Ishak Hashim[6] · Roohollah Babaei Mahani[7,8]

Received: 29 May 2020 / Accepted: 21 September 2020

Abstract

In the present study, the free convection heat transfer of a power-law non-Newtonian fluid is considered in a cavity containing a flexible hot thin heater. The sidewalls of the square cavity are maintained at cold temperatures, while the hot heater is placed inside the cavity. The top and bottom walls of the cavity are kept insulated. The thin heater plate can undergo large deformations due to the interaction between the fluid flow and the heater. The arbitrary Lagrangian–Eulerian moving mesh method is employed to track the displacement of the heater in the fluid domain. Appropriate non-dimensional parameters are utilized to transform the governing equations into a general non-dimensional form. The equations governing fluid flow and heat transfer are solved using the finite element method with an automatic time-stepping scheme. The effect of control parameters such as the non-Newtonian power index ($0.6 < n < 1.4$), the Rayleigh number ($10^4 < \mathrm{Ra} < 10^6$), the element location and length is studied on the hydraulic and thermal behavior of the cavity and element displacement. The results indicate that raising the power-law index (n) from the pseudoplastic behavior ($n < 1$) to the dilatant ($n > 1$) behavior reduces the fluid circulation and heat transfer rate in the cavity, but it increases the magnitude of the exerted tensions on the element. Moreover, raising Ra from 10^4 to 10^6 enhances the average heat transfer the value of $\mathrm{Nu}_{\mathrm{av}}$ by up to 3.5 times in pseudoplastic fluids and by 1.5 times in dilatant ones. In addition, it is found that shifting the heater upward deteriorates the heat transfer rate by suppressing the convection flow intensity. A 35% rise in the average heater can be obtained when the height of the plate was divided by 4 in the cse of dilatant fluid, and an increase by up to 100% is found for pseudoplastic fluids. Increasing the length of the element is also found to reduce the average Nusselt number and to increase the tensions in the heater. The average Nusselt number can be doubled when the length of the plate is reduced seven times.

Keywords Fluid–structure interaction (FSI) · Power-law non-Newtonian fluid · Natural convection heat transfer · Arbitrary Lagrangian–Eulerian (ALE) moving mesh

List of symbols

c_{p}	The isobaric specific heat capacity
$\boldsymbol{D}$	The structure displacement
E	Dimensional Young's modulus
E_{τ}	Non-dimensional elasticity modulus
$\mathbf{g}$	Gravitational acceleration

✉ Roohollah Babaei Mahani
roohollahbabaeimahani@duytan.edu.vn

Mohammad Ghalambaz
mohammad.ghalambaz@tdtu.edu.vn

[1] Metamaterials for Mechanical, Biomechanical and Multiphysical Applications Research Group, Ton Duc Thang University, Ho Chi Minh City, Vietnam

[2] Faculty of Applied Sciences, Ton Duc Thang University, Ho Chi Minh City, Vietnam

[3] Young Researchers and Elite Club, Yasooj Branch, Islamic Azad University, Yasooj, Iran

[4] Department of Mechanical Engineering, Shahrekord University, Shahrekord, Iran

[5] LabECAM, ECAM Lyon, Université de Lyon, Lyon, France

[6] Department of Mathematical Sciences, Faculty of Science and Technology, Universiti Kebangsaan Malaysia, 43600 UKM Bangi, Selangor, Malaysia

[7] Institute of Research and Development, Duy Tan University, Da Nang 550000, Vietnam

[8] Faculty of Civil Engineering, Duy Tan University, Da Nang 550000, Vietnam

Published online: 27 November 2020

G_v Exerted body force
L Height of the enclosure
P Pressure field
Pr Prandtl number
Ra Rayleigh number
t Time
T Fluid and solid temperatures
$\boldsymbol{u}$ Fluid velocity vectors
$\boldsymbol{w}$ Moving mesh velocity vectors
x, y Cartesian coordinates

Greek symbols

α The fluid's thermal diffusivity
β Coefficient of thermal expansion
ι, λ Structure modules defined in Eq. (7)
μ Viscosity of the fluid in the enclosure
ν Poisson's ratio
ν_f Kinematic viscosity
ρ Density for fluid and the structure
ρ_r The density of the fluid to that of the structure
σ Stress tensor
τ Dimensionless time

Subscripts

av Average
c, h Cold and hot temperatures
f The fluid in the enclosure
s Flexible thin plate

Superscripts

tr Matrix transpose operator
* The dimensional form

Introduction

Convection in a differentially heated cavity is an important problem in many engineering applications such as biomechanics, automotive, MEMS, and aerospace. Fluid–structure interaction (FSI) has received considerable attention in recent years due to its potential applications in heat transfer enhancement. Various aspects of natural convection heat transfer in enclosures such as conjugate heat transfer [1, 2], using nanofluids [3], hybrid nanofluids [4], and porous media [5] have been addressed in recent years.

Considering FSI effects, Al-Amiri and Khanafer [6] explored the effect of a right vertical flexible wall on natural convection in a porous cavity. Khanafer [7] was most probably the first to study the effect of a flexible bottom surface on convective flow in a differentially-heated cavity. The outcomes of both studies showed that the elasticity of the flexible wall could have a significant impact on heat transfer enhancement. Khanafer [8] exhibited that the rate of heat transfer can be enhanced significantly by the flexible bottom wall for the case of a high value of the Grashof number and a moderate Reynolds number. Investigations of FSI in heated 2D channel flow problems having thin, flexible plates/flaps can be found in [9–11], which showed heat transfer performance enhancement. There are also some studies which addressed the interaction of flexible structured immersed in fluids [12–14].

Selimefendigil et al. [15] examined the combined effects of a flexible right wall and an inner rotating cylinder on mixed convection of a nanofluid in a cavity. Selimefendigil and Oztop [16] considered convection in a nanofluid-filled cavity having two flexible walls and an inner rotating cylinder. The heat transfer inside the cavity was found to be controlled by the flexible sidewalls. Selimefendigil and Oztop [17] considered a cavity with a flexible right wall and filled with CuO–water nanofluid under the influence of an inclined magnetic field and volumetric heat generation. They showed that increasing the Richardson and Hartmann and internal Rayleigh numbers reduces the averaged heat transfer.

Alsabery et al. [18] studied the combined effects of a flexible wall and an inner heated rotating cylinder on convection and entropy generation in a cavity. Anticlockwise rotation of the cylinder and small wall deformation gives a high heat transfer rate. Alsabery et al. [19] analyzed transient convection in a cavity with a partially heated left wall, a right flexible wall and having an inner cylinder. Raising the flexibility of the slanted wall of a triangular cavity and nanoparticle concentration enhances the heat transfer, as found by Selimefendigil and Oztop [20]. Selimefendigil et al. [21] studied the effects of a flexible right wall, an inclined magnetic field, and a moving top wall on convection in a nanofluid-filled cavity. Convection in an inclined 3D trapezoidal cavity having two flexible walls was investigated by Selimefendigil et al. [22].

Convection problems in a cavity having a flexible structure positioned within it are important too since the presence of the flexible fin affects both the flow and thermal fields within the cavity. Jamesahar et al. [23] examined convection in a square cavity diagonally partitioned by a thin flexible membrane. The heat transfer was found to be higher than that of the solid membrane. In another study, Mehryan et al. [24] studied unsteady MHD convection in a cavity partitioned by a thin flexible membrane. They found that the induced stresses in the membrane can be affected by the magnetic field. An inclined version of the problem with a sinusoidal temperature of the right wall and without the magnetic field was analyzed by Mehryan et al. [25]. The effect of the sinusoidal temperature condition on the membrane was found to be negligible.

The effect of the sinusoidal temperature condition on the membrane was found to be negligible. Alshuraiaan and Khanafer [26] found that a horizontal porous thin fin attached to a wall of a cavity could increase heat transfer.

Ali et al. [27] showed that heat transfer could be improved in a 2D channel flow using freely oscillating flexible flaps. Ghalambaz et al. [28] examined the effect of a flexible fin attached to the left wall of a cavity. They found a significant improvement in heat transfer enhancement by increasing the amplitude of the fin oscillation.

Ismael and Jasim [29] considered convection in a cavity having an inlet (at the bottom of the left wall) and an outlet (at the top of the right wall) openings. A flexible fin placed close to the inlet opening was found to enhance the heat transfer. Alsabery et al. [30] studied the effect of a flexible oscillating fin on convection in a partially heated oblique cavity. They found that the heat transfer rate can be improved when the oscillation amplitude of the flexible fin's end is increased. Selimefendigil et al. [31] examined the combined effects of a flexible fin attached to the cavity's top wall, an inclined magnetic field, and moving left wall on convection of a nanofluid. Again, decreasing the rigidity of the flexible fin has the effect of increasing the heat transfer.

Yaseen and Ismael [32] considered mixed convection of a non-Newtonian fluid in a 2D open trapezoidal cavity with a parallel plane channel and a flexible fin attached to the top wall. They found the presence of the flexible fin has a negligible effect on the heat transfer performance. Sabbar et al. [33] studied the mixed convection heat transfer in a channel with a rectangular expanded section and flexible wall. The results show that the presence of a flexible wall could improve the heat transfer by 17% compared to a rigid wall. Sun et al. [34] showed that heat transfer from a circular cylinder could be enhanced significantly by a flexible heated fin attached to the cylinder. The presence of elastic walls could improve or deteriorate the heat transfer rate. Selimefendigil and Oztop [35] simulated the mixed convection flow and heat transfer in a channel with two flexible walls.

Saleh et al. [36] recently investigated the effects of two flexible fins attached to the top wall of a cavity. They found that the same-direction and the opposite-direction oscillations of the fins give different instantaneous heat transfer characteristics. Raisi and Arvin [37] considered an FSI problem where an adiabatic flexible baffle was placed at the center of a cavity having a flexible top wall. Zadeh et al. [38] showed that increasing the baffle length has mixed effects on the thermal performance of the system. An increase in the baffle's flexibility reduces the Nusselt number. Mehryan et al. [39] examined the effect of the presence of an inclined flexible baffle in an enclosure. The baffle could be fixed at its center or its edges. The results revealed that the fixed location of the baffle induces a notable impact on the baffle deformation and heat transfer. The flexible baffles are also employed for natural convection flow control in a cavity [40]. Khanafer and Vafai [36] presented a good review of FSI in porous media recently.

The natural convection heat transfer of non-Newtonian fluids in FSI applications has not received much attention yet. In the present work, we shall examine the influence of the heated thin plate on the convective heat transfer of a non-Newtonian fluid in the cavity.

Problem mathematical formulation

The current work investigates natural convection heat transfer of a power-law non-Newtonian fluid occupying a square cavity containing a horizontally placed flexible thin heater. The sidewalls of the cavity are maintained at a cold temperature T_c^*, whereas the top and bottom sidewalls are assumed thermally insulated. However, the flexible heater is maintained at a hot temperature T_h^*. All of the cavity sidewalls are assumed stationary and impermeable, and the no-slip condition applies to all of them. Figure 1 illustrates the schematic diagram and the coordinate system of the problem. The enclosure is a square with a size of L^*. The flexible thin plate is assumed isotropic and uniform with a thickness t_p^*. All thermophysical properties are assumed constant except the density variation in the momentum equations, which is estimated by Boussineq's approximation. The force of gravity is taken into account and directed vertically, and the body forces on the thin plate include its mass and the buoyancy force.

Based on the physics of the problem, the governing equations include the balance laws of mass, linear momentum, and energy. Taking into account all of the above assumptions, and employing the arbitrary Lagrangian–Eulerian (ALE) technique, the governing equations can be written as [41]:

Continuity equation:

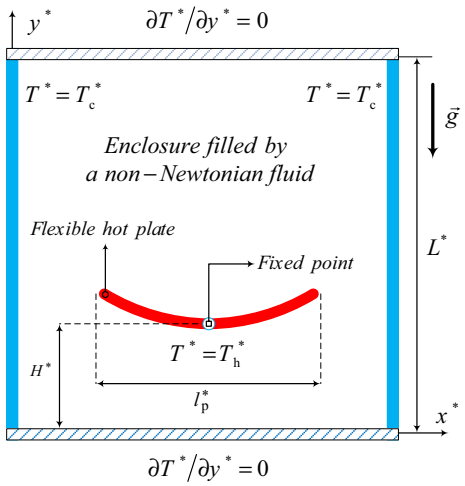

Fig. 1 Schematic diagram of the problem

$$\nabla^* \cdot \mathbf{u}^* = 0 \tag{1}$$

Linear momentum equations:

$$\rho_f\left[\frac{\partial \mathbf{u}^*}{\partial t} + (\mathbf{u}^* - \mathbf{w}^*)\cdot\nabla^*\mathbf{u}^*\right] = \nabla^*\cdot\left[-P^*I + \mu\left(\nabla^*\mathbf{u}^* + (\nabla^*\mathbf{u}^*)^{tr}\right)\right] + \rho_f\beta\mathbf{g}\left(T^* - T_c^*\right) \tag{2a}$$

in which

$$\mu(\dot{\gamma}) = m\mu_a \left| \begin{array}{l} \mu_a = (\dot{\gamma})^{n-1} \\ \dot{\gamma} = \max\left(\sqrt{[\mathbf{D}^*] : [\mathbf{D}^*]}, \dot{\gamma}_{min}\right) \\ 2\mathbf{D}^* = \nabla\mathbf{u}^* + (\nabla\mathbf{u}^*)^{tr} \end{array} \right. \tag{2b}$$

where m and n denote the non-Newtonian fluid consistency coefficient and the power-law index, respectively. It should be noted that for $n<1$, the non-Newtonian fluid is called pseudoplastic fluid whereas for $n>1$, the non-Newtonian fluid is called dilatant fluid. However, when $n=1$, the Newtonian fluid condition is recovered. These classifications are well known and are based on the changes in the apparent viscosity as a result of increasing shear stress. For a pseudoplastic fluid, the apparent viscosity decreases as the shear rate increases, whereas it augments with increases in the shear rate for a dilatant fluid.

Energy equation:

$$\left(\rho c_p\right)_f\left(\frac{\partial T^*}{\partial t} + (\mathbf{u}^* - \mathbf{w}^*)\cdot\nabla^* T^*\right) = k_f\nabla^{*^2}T^* \tag{3}$$

The nonlinear elastodynamic equation of the flexible plate:

$$\rho_s\frac{\mathrm{d}^2\mathbf{d}_s^*}{\mathrm{d}t^2} - \nabla^*\boldsymbol{\sigma}^* = G_v^* \tag{4}$$

where $\mathbf{w}^* = \left(u_s^*, v_s^*\right)$ represents the velocity vector the moving grid, $\mathbf{u}^* = (u^*, v^*)$ accounts for the vector of the fluid velocity, P^* indicates the fluid pressure, T^* is the solid/fluid temperature, $\mathbf{g}$ denotes the acceleration due to gravity, and c_p is the specific heat capacity. The subscripts f and s indicate the fluid and the structure, respectively. $\mathbf{d}_s^*$ is the thin plate displacement vector such that $\mathrm{d}\mathbf{d}_s^*/\mathrm{d}t = \mathbf{w}^*$, $\boldsymbol{\sigma}^*$ is the solid stress tensor, and G_v^* represents the body force exerted on the thin plate. It should be noted that the stress analyzed here is the von Mises stress, and it is monitored over the entire fin surface. However, since the basis of the fin at the surface is the point where maximum strain occurs, the maximum will also be on the boundary of the fin. The density is represented by ρ with subscripts f and s corresponding to the fluid and solid, respectively. The symbols of ν_f, and β denote the fluid kinematic viscosity, thermal diffusivity, and the volumetric thermal expansion coefficient, respectively. Finally, the thermal diffusivity is depicted by $\alpha_f = k_f/(\rho \times C_p)_f$. The stress tensor in Eq. (4) is represented by the Neo-Hookean solid model as follows:

$$\boldsymbol{\sigma}^* = J^{-1}FSF^{tr} \tag{5}$$

where F^{tr} denotes the transpose of matrix F and the symbol S is the Piola–Kirchhoff stress tensor and is linked to the strain energy density function W_s and the strain ε by the following equations:

$$F = \left(I + \nabla^*\mathbf{d}_s^*\right),\quad J = \det(F) \text{ and } S = \partial W_s/\partial\varepsilon \tag{6}$$

$$W_s = \frac{1}{2}\ell\left(J^{-1}I_1 - 3\right) - \ell\ln(J) + \frac{1}{2}\lambda(\ln(J))^2 \left| \begin{array}{l} \iota = E/(2(1+\nu)) \\ \lambda = E\nu/((1+\nu)(1-2\nu)) \end{array} \right. \tag{7}$$

$$\varepsilon = \frac{1}{2}\left(\nabla^*\mathbf{d}_s^* + \nabla^*\mathbf{d}_s^{*tr} + \nabla^*\mathbf{d}_s^{*tr}\nabla^*\mathbf{d}_s^*\right) \tag{8}$$

The interface boundary conditions between the non-Newtonian fluid and the hot plate and those on the boundaries are as follows:

$$\text{On the side walls}: \quad T^* = T_c^*,\quad u^* = v^* = 0 \tag{11a}$$

$$\text{On the top and bottom walls}: \quad \frac{\partial T^*}{\partial y^*} = 0,\quad u^* = v^* = 0 \tag{11b}$$

Also, those on the surfaces of the flexible hot plate are given by

$$\boldsymbol{\sigma}^*\cdot n = -P^* + \mu(\dot{\gamma})\nabla^*\mathbf{u}^*,\quad T^* = T_h^*,\quad \frac{\partial\mathbf{d}_s^*}{\partial t} = \mathbf{u}^* \tag{11c}$$

The governing partial differential Eqs. (1)–(4) are non-dimensionalized by employing the following dimensionless parameters:

$$\mathbf{d}_s = \frac{\mathbf{d}_s^*}{L^*},\ \boldsymbol{\sigma} = \frac{\boldsymbol{\sigma}^*}{E},\ \tau = \frac{t\alpha_f}{L^{*2}},\ (x, y, H, t_p, l_p) = \frac{(x^*, y^*, H^*, t_p^*, l_p^*)}{L^*}$$
$$\mathbf{u} = \frac{\mathbf{u}^*L^*}{\alpha_f},\ \mathbf{w} = \frac{\mathbf{w}^*L^*}{\alpha_f},\ P = \frac{P^*L^{*2}}{\rho_f\alpha_f^2},\ T = \frac{T^* - T_c^*}{T_h^* - T_c^*},\ \nabla = \nabla^*L^* \tag{12}$$

to yield the following dimensionless equations:

$$(\nabla\cdot\mathbf{u}) = 0 \tag{13}$$

$$\frac{\partial\mathbf{u}}{\partial\tau} + (\mathbf{u} - \mathbf{w})\cdot\nabla\mathbf{u} = \nabla\cdot\left[-PI + \mathrm{Pr}\dot{G}^{n-1}(\nabla\mathbf{u} + (\nabla\mathbf{u})^{tr}\right] + \mathrm{PrRa}T\mathbf{j} \tag{14}$$

where

$$\dot{G} = \max\left(\sqrt{[\mathbf{D}] : [\mathbf{D}]}, \dot{G}_{\min}\right) |2\mathbf{D} = \nabla\mathbf{u} + (\nabla\mathbf{u})^{\mathrm{tr}} \tag{15}$$

Also, the Rayleigh and Prandtl numbers are defined as:

$$\mathrm{Ra} = \frac{g\beta\left(T_h^* - T_c^*\right)L^{*3}}{\upsilon_f \alpha_f}, \quad \mathrm{Pr} = \frac{\upsilon_f}{\alpha_f} \tag{16}$$

$$\frac{\partial T}{\partial \tau} + (\mathbf{u} - \mathbf{w}) \cdot \boldsymbol{\nabla} T = \boldsymbol{\nabla}^2 T \tag{17}$$

$$\frac{1}{\rho_r}\frac{\mathrm{d}^2\mathbf{d}_s}{\mathrm{d}\tau^2} - E_\tau \boldsymbol{\nabla}\boldsymbol{\sigma} = E_\tau G_v \tag{18}$$

where

$$E_\tau = \frac{EL^{*2}}{\rho_f \alpha_f^2}, \; G_v = \frac{\left(\rho_f - \rho_s\right)L^*\mathbf{g}}{E}, \; \rho_r = \frac{\rho_f}{\rho_s} \tag{19}$$

Here, the exerted buoyancy force inside the plate was ignored (i.e., $\boldsymbol{G}_\nu = 0$). The non-dimensional boundary conditions can be written as

$$\text{On the sidewalls} : T = 0, \quad u = v = 0 \tag{20a}$$

$$\text{On the top and bottom} : \frac{\partial T}{\partial y} = 0, \quad u = v = 0 \tag{20b}$$

The dimensionless form of the boundary conditions at the fluid–plate interface becomes as follows:

$$\boldsymbol{\sigma} \cdot n = -P + \mathrm{Pr}\dot{G}^{n-1}\boldsymbol{\nabla}\mathbf{u}, T = 1, \quad \frac{\partial \mathbf{d}_s}{\partial t} = \mathbf{u} \tag{20c}$$

The initial conditions for the dimensionless fluid velocity and pressure are such that they are both null, whereas the initial dimensionless temperature is equal to 0.5. The local Nusselt number on the flexible hot thin element is assumed to represent the heat transfer rate as:

$$\mathrm{Nu}_{\mathrm{local}} = -\left.\frac{\partial T}{\partial n}\right|_{\text{On the hot plate}} \tag{21}$$

where n denotes the direction normal to the flexible plate's surface. The average Nusselt number is calculated by integration of the local Nusselt number over the hot thin plate boundaries as follows:

$$\mathrm{Nu}_{\mathrm{avg}} = \frac{1}{2\left(l_p + t_p\right)} \int_{\text{Hot plate}} \mathrm{Nu}_{\mathrm{local}} \mathrm{d}s \tag{22}$$

Ultimately, the following partial differential equation is solved to visualize the flow patterns of the fluid:

$$\boldsymbol{\nabla}^2 \psi = -\boldsymbol{\nabla} \times \mathbf{u} \tag{23}$$

The value of ψ, namely stream function, on the outer walls of the enclosure, is zero.

Numerical solution and validations

Numerical approach

Due to the complexity of equations coupled with the boundary conditions, it requires to convert them to a weak form of equations. After the conversion, the Galerkin finite element method accompanied by the ALE technique is applied to solve the weak equations. The details of the Galerkin method are available in Ref. [42]. The Yeoh scheme, with a stiffness factor of 100, was used for mesh smoothing. The equations were solved in fully coupled from, and the time step was controlled automatically employing the backward differentiation formula.

Grid study and independence test

As shown in Fig. 2, a non-structured triangular mesh is provided for the computational domain of study, while a condensed structured mesh is applied for the plate. In order to assure that the quality of the grids used in the study is acceptable, the grid independence examination is an important step. The grid independence test is accomplished in a way that the variations in the average Nusselt number,

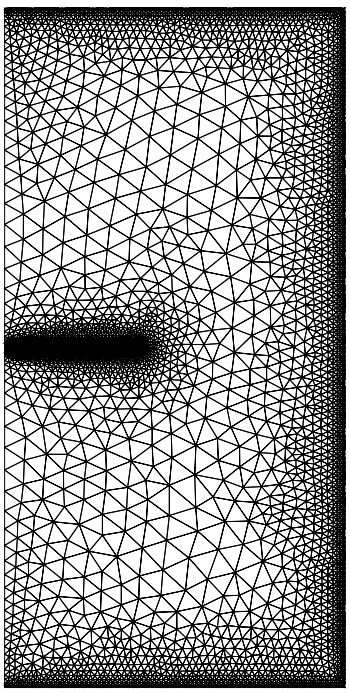

Fig. 2 Sample of utilized mesh

Table 1 Mesh independency based on Ra = 10^6, Pr = 10, $E_\tau = 5\times10^9$, $n = 0.6$

Mesh elements	Nu_{av}	σ_{max}	$\lvert\Psi\rvert_{max}$
2191	27.658	8.2788E8	79.00
3331	27.818	8.1471E8	83.086
5199	28.225	7.9255E8	87.925
7509	28.274	7.9395E8	88.650
9511	**28.327**	**7.9313E8**	**90.802**
12,840	28.433	7.9585E8	90.500

The bold element size was adopted for the computation of the results

maximum stress, and maximum strength of the streamlines become negligible with the increasing the number of the elements. Table 1 shows the variations in these parameters versus the element numbers. It can be seen that the acquired results for 9511 and 12,840 number of elements have a slight difference. Thus, due to lessen the computational costs, the mesh elements number of 9511 was chosen for numerical simulations.

Comparisons with others

A vital part of numerical studies is to demonstrate the accuracy and correctness of the results by comparison with other studies. To verify the deformation of the flexible wall, the results of this study were compared with Kuttler and Wall [43] research. They did investigations on a lid-driven cavity equipped with a flexible wall. According to Fig. 3a, the deformation of the flexible wall of the cavity in this study and Ref. [43] shows a good agreement. In order to examine the verification of natural convection mechanism for non-Newtonian fluid in this study, the obtained FSI code of this study was used to re-simulate the Matin and Khan [44] numerical study. They examined the natural convection heat transfer of a non-Newtonian fluid inside a cavity. As shown in Fig. 3b, an excellent agreement is evident between these two studies. Finally, the average Nusselt number and maximum stream function magnitude of this study and Ref. [45] were compared at various values of Rayleigh numbers. They addressed the natural convection heat transfer mechanism in an air-filled square cavity in which a plate was placed horizontally or vertically. It can be seen in Table 2 that the range of difference between the two studies is 0.49–4.2%, which verifies the results of this research.

Results

Here, the impacts of various parameters on fluid flow and heat transfer in the cavity are analyzed. These following parameters are considered: Rayleigh number

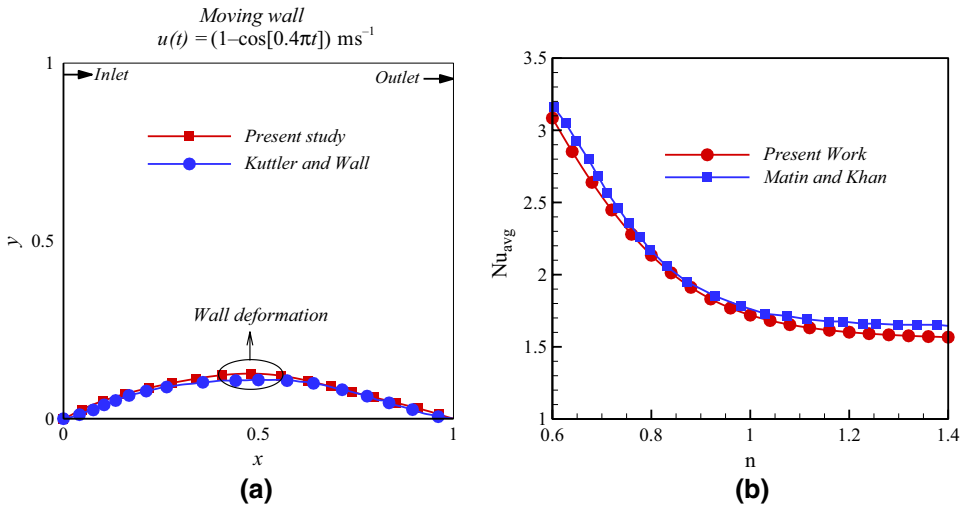

Fig. 3 **a** Comparison of the wall deformation between the present study and the result of Kuttler and Wall [43]; **b** the average Nusselt number against power-law index n of the current study and Matin and Khan (points) [44]

Table 2 Average Nusselt numbers and $|\psi_{max}|$, and comparison between the present study and the result of Saravanan and Sivaraj [45] considering the zero wall emissivity and $l_p = 0.5$

Ra	1E5		1E6		10E7	
	$\lvert\psi_{max}\rvert$	Nu_{av}	$\lvert\psi_{max}\rvert$	Nu_{av}	$\lvert\psi_{max}\rvert$	Nu_{av}
Present study	7.0928	3.2774	15.471	5.1558	32.6441	8.4297
Saravanan and Sivaraj [45]	7.0358	3.3339	15.5904	5.2804	32.4851	8.7997
Error (%)	0.81	1.69	0.77	2.36	0.49	4.20

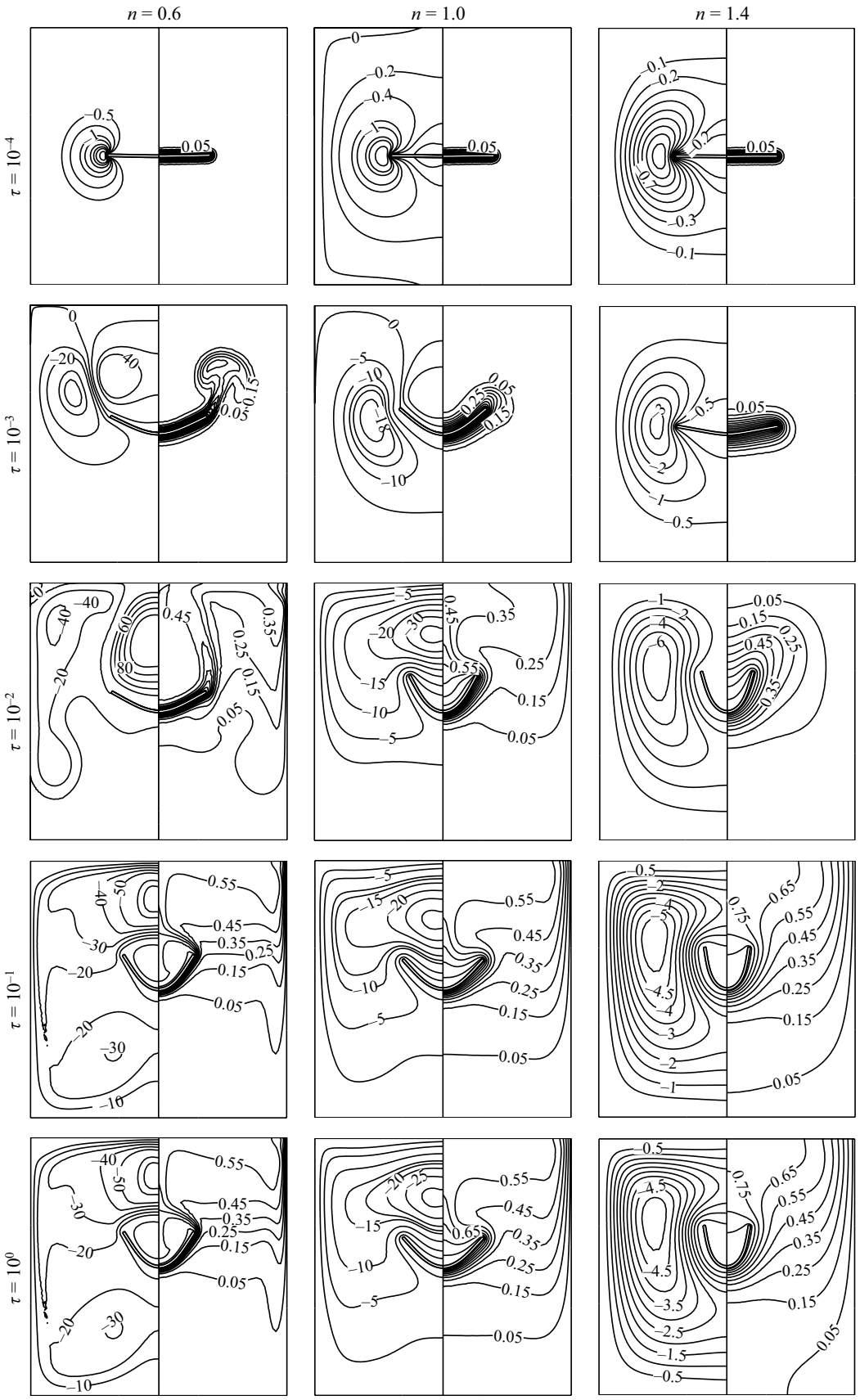

Fig. 4 Time variation of isotherms (right) and streamlines (left) at $H = 0.5$, $l_p = 0.4$, $\mathrm{Ra} = 10^6$, $\mathrm{Pr} = 10$, and $E_\tau = 10^{10}$

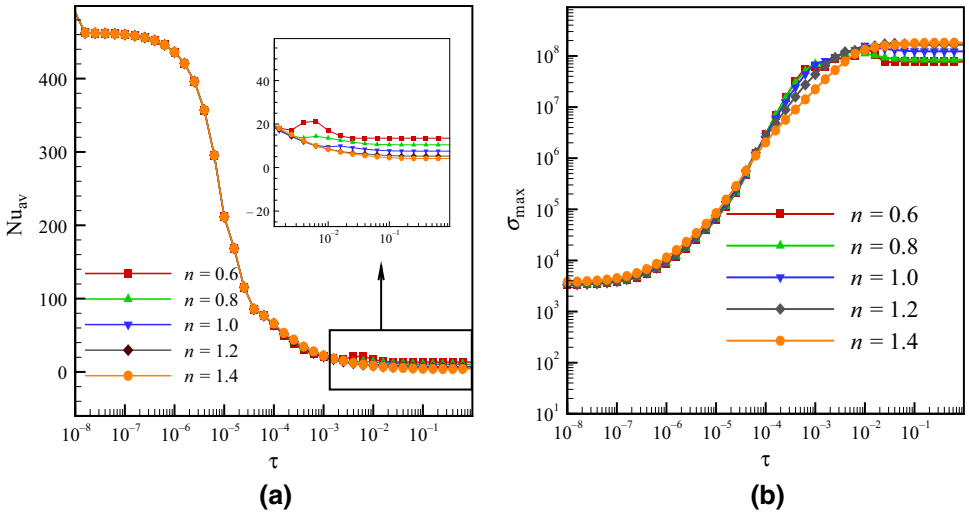

Fig. 5 Effect of the power-law index (n) during the time on **a** the average Nusselt number (Nu_{av}), and **b** σ_{max} in the plate when $Ra = 10^5$, $Pr = 10$, $E_\tau = 10^{10}$, $H = 0.5$, and $l_p = 0.4$

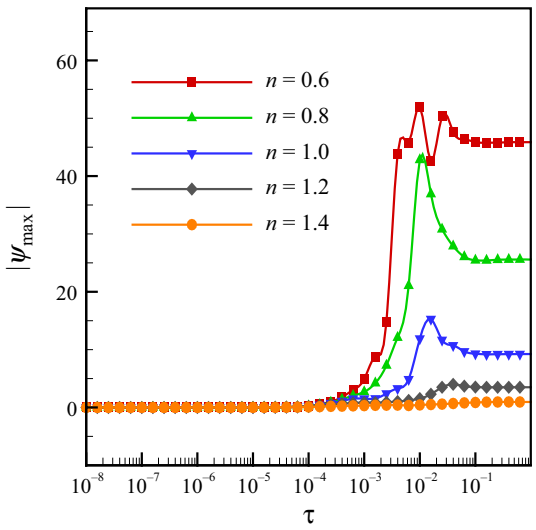

Fig. 6 Effect of the power-law index (n) during the time on maximum streamline $|\psi_{max}|$ when $Ra = 10^5$, $Pr = 10$, $E_\tau = 10^{10}$, $H = 0.5$, and $l_p = 0.4$

($10^4 \le Ra \le 10^6$), power-law index ($0.6 \le n \le 1.4$), plate length ($0.1 \le l_p \le 0.7$), elasticity modulus ($5 \times 10^9 \le E_\tau \le 5 \times 10^{11}$), and the distance between the bottom wall and the thin plate center ($0.3 \le H \le 0.7$). The other parameters remained constant throughout the analysis, like the density ratio ($\rho_r = 1$) and the plate thickness ($t_p = 0.01$).

Figure 4 illustrates the development of streamlines and of the isotherms in the enclosure with time for various values of the fluid power-law index, i.e., n. It is shown that initially, the streamlines are more developed for $n = 1$, compared to the two other cases. As time goes, the flow becomes more developed for $n = 0.6$ due to a lower resistive shear stresses in the case of a pseudoplastic fluid. For that case, a recirculation zone appears near the bottom of the cavity. For $n = 1$, the flow is slow, and the streamlines surround the flexible plate. For a dilatant fluid ($n = 1.4$), the first observation is that the flexible plate is more inclined than the two other cases. For the case of dilatant fluid, although the flow velocity is low, the shear stresses of the fluid are higher, and this is why the deflection of the flexible plate is more for $n = 1.4$. Also, it can be seen that the streamlines are concentric curves having the center above the cavity middle. As for the isotherms, it is clear that the contours shape is similar in the three cases. However, the contours of each temperature are slightly higher for lower n, indicating that the fluid is hotter in the upper part of the cavity. The decrease in the resistive shear stress when n is decreased intensifies the convective flow leading to this distribution of the isothermal contours.

The variation in the maximum stress (σ_{max}) and the average Nusselt number (Nu_{av}) as functions of time for different values of n is plotted in Fig. 5. The value of n slightly affects the variations of Nu_{av} and σ_{max}. For the former, in the steady part of the curve, the value of Nu_{av} is higher for $n = 0.6$ than the other cases and it is minimum for $n = 1.4$. Indeed, the apparent viscosity increases for higher values of n and leads to higher flow resistance. This limitation in convective flow translates into a decrease in the heat transfer by convection, as indicated by the reduction of Nu_{av}. On the other hand, this increase in the apparent viscosity raises the magnitude of the hydrodynamic interaction force between the fluid and the baffle and increases σ_{max}, which is at its highest for $n = 1.4$ and decreases when n is reduced.

The effect of n on the variation in the absolute value of the maximum of the stream function $|\psi_{max}|$ as a function of time is shown in Fig. 6. $|\psi_{max}|$ increases substantially when n is decreased and is at its highest for $n = 0.6$, while it is slightly greater than zero for $n = 1.2$. $|\psi_{max}|$ is an indicator of the strength of the fluid flow. When the apparent viscosity is reduced for $n < 1$ in the case of a pseudoplastic

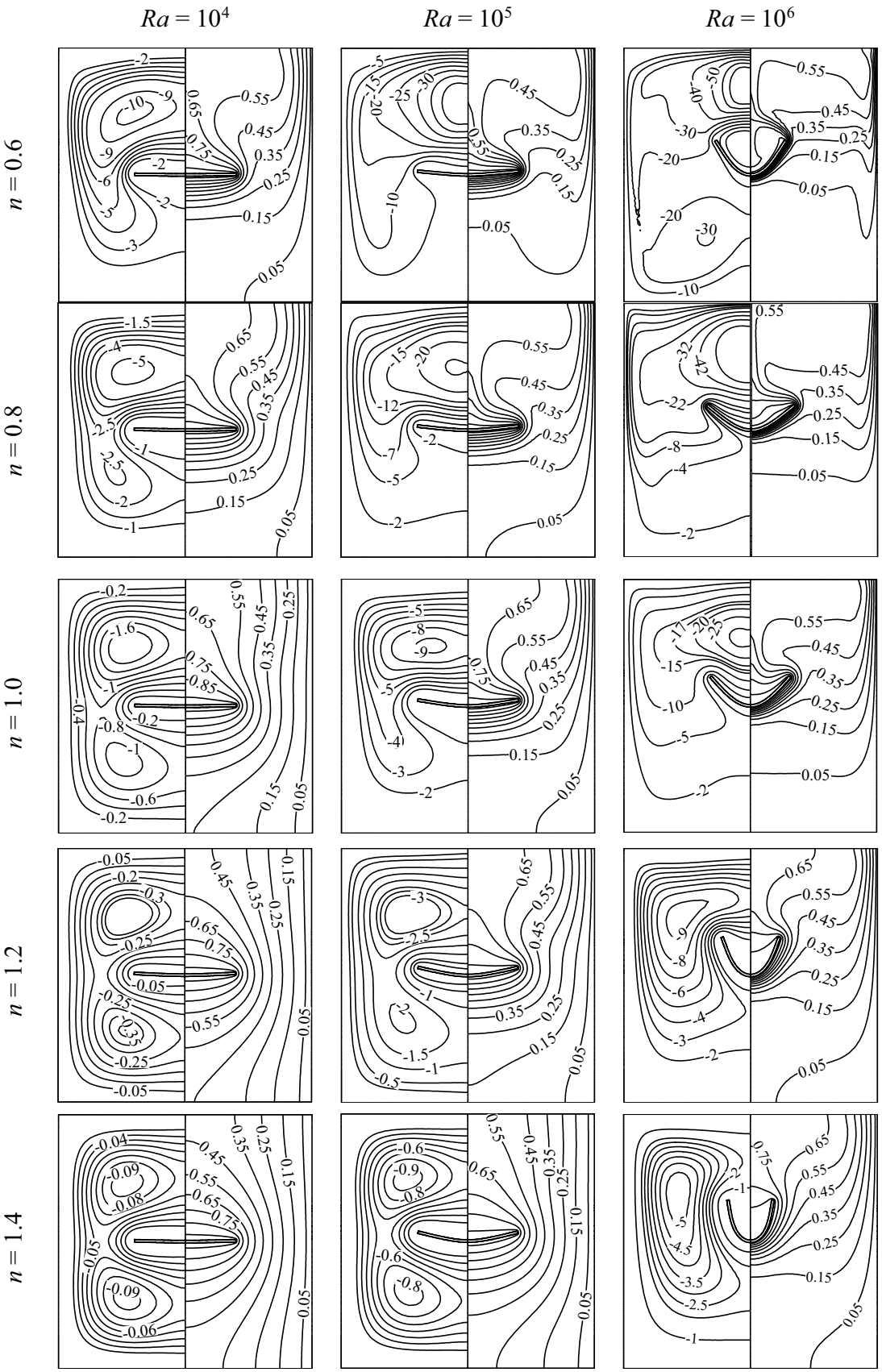

Fig. 7 Effect of n and Rayleigh number on the isotherm and streamlines based on $H=0.5$, $l_p=0.4$, $\mathrm{Pr}=10$, $E_\tau=10^{10}$

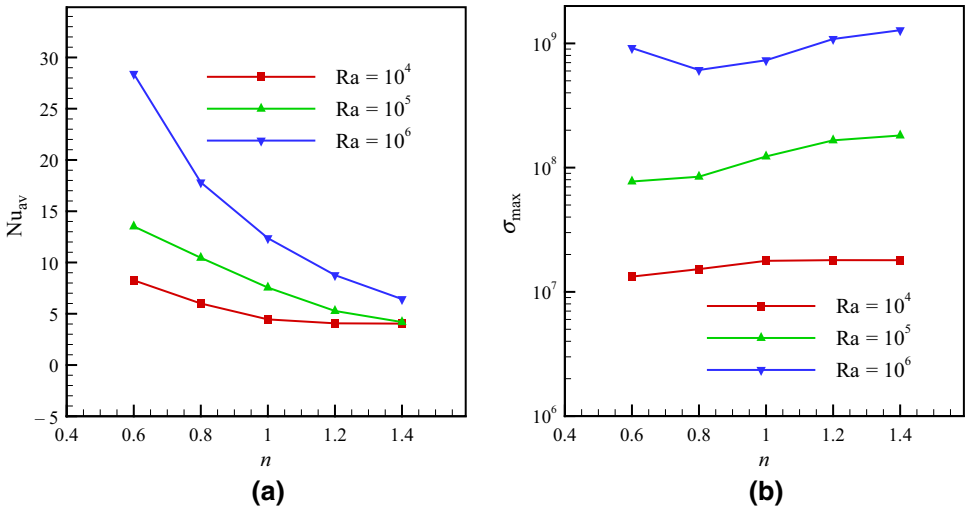

Fig. 8 Variations of **a** average Nusselt number (Nu_{av}) and **b** the maximum plate stress (σ_{max}) for selected values of Ra at Pr = 10, $E_\tau = 10^{10}$, $H = 0.5$, and $l_p = 0.4$

(shear-thinning) fluid, the flow faces less resistance from the flow, and its strength increases. The exact opposite occurs in the case of a dilatant (shear-thickening) fluid, where the flow strength is reduced. The change in the strength of the flow with n is equivalent to a change of the intensity of convection as discussed in Fig. 5.

Figure 7 depicts the streamlines and the isotherms in the enclosure for selected Rayleigh numbers (Ra) and the power-law index (n). For $n = 0.6$, increasing Ra from 10^4 to 10^6 increases the magnitude of the velocity, and an additional vortex appears below the plate. The streamlines also tend to cover a greater surface inside the cavity. A similar trend can be observed for $n = 0.8$, but with a lower velocity magnitude. In the case of a Newtonian fluid ($n = 1$), a vortex below the plate appears for $Ra = 10^4$ and vanishes when the velocity

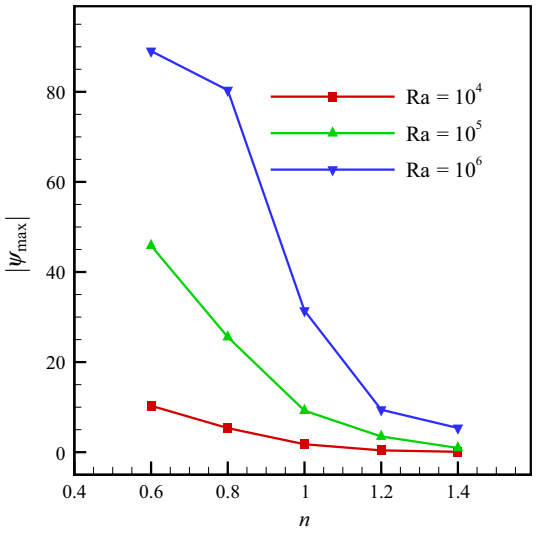

Fig. 9 Variation in maximum streamline $|\psi_{max}|$ for different power-law index (n) at different Ra at $l_p = 0.4$, $H = 0.5$, Pr = 10, $E_\tau = 10^{11}$, and $Ra = 10^6$

increases for higher Ra. Further increasing n reduces the effect of Ra on the streamline patterns. This is due to the fact that increasing n raises the apparent viscosity of the fluid. As Ra indicates the relative significance of the buoyancy forces with respect to the viscous forces, its effect becomes less apparent when n is increased, i.e., when the resistive viscous forces in the flow intensify. For instance, comparing the cases $Ra = 10^4$ and $Ra = 10^5$ for $n > 1$ shows a similar flow pattern. A similar pattern can also be seen when comparing the cases $n = 1.2$ and $n = 1.4$ for $Ra = 10^6$. However, the flow velocity magnitude is increased when Ra is raised or when n is reduced. As for the isotherms, increasing Ra tends to raise the position of low-temperature isotherms inside the enclosure, due to enhanced convection effects as observed in the flow patterns. Nonetheless, these effects become less apparent for higher values of n when the viscous forces are relatively more important.

The variations of Nu_{av} and σ_{max} as functions of n for different values of Ra are shown in Fig. 8. It can be seen that for all the values of n, Nu_{av} increases with the rise of Ra. Nonetheless, this increase is less apparent for higher values of n. For instance, for $n = 1.4$, increasing Ra from 10^4 to 10^5 has little effect on the value of Nu_{av} due to the presence of important resistive viscous forces in the flow compared to the other cases. Raising Ra from 10^4 to 10^6 increases 3.5 times the value of Nu_{av} for $n = 0.6$ and by 1.5 times for $n = 1.4$. Indeed, Ra represents the relative importance of buoyancy forces with respect to the resistive viscous forces, and increasing its value raises the natural convection effects and, consequently, the convective heat transfer. A similar observation can be noted for the value of σ_{max}, which increases with Ra for all the values of n. The order of magnitude of the increase is around 10 when the value of Ra is increased ten times. When the convective effects are increased, the flow acts over the plate with a higher interaction force, which, as a consequence, increases the resulting

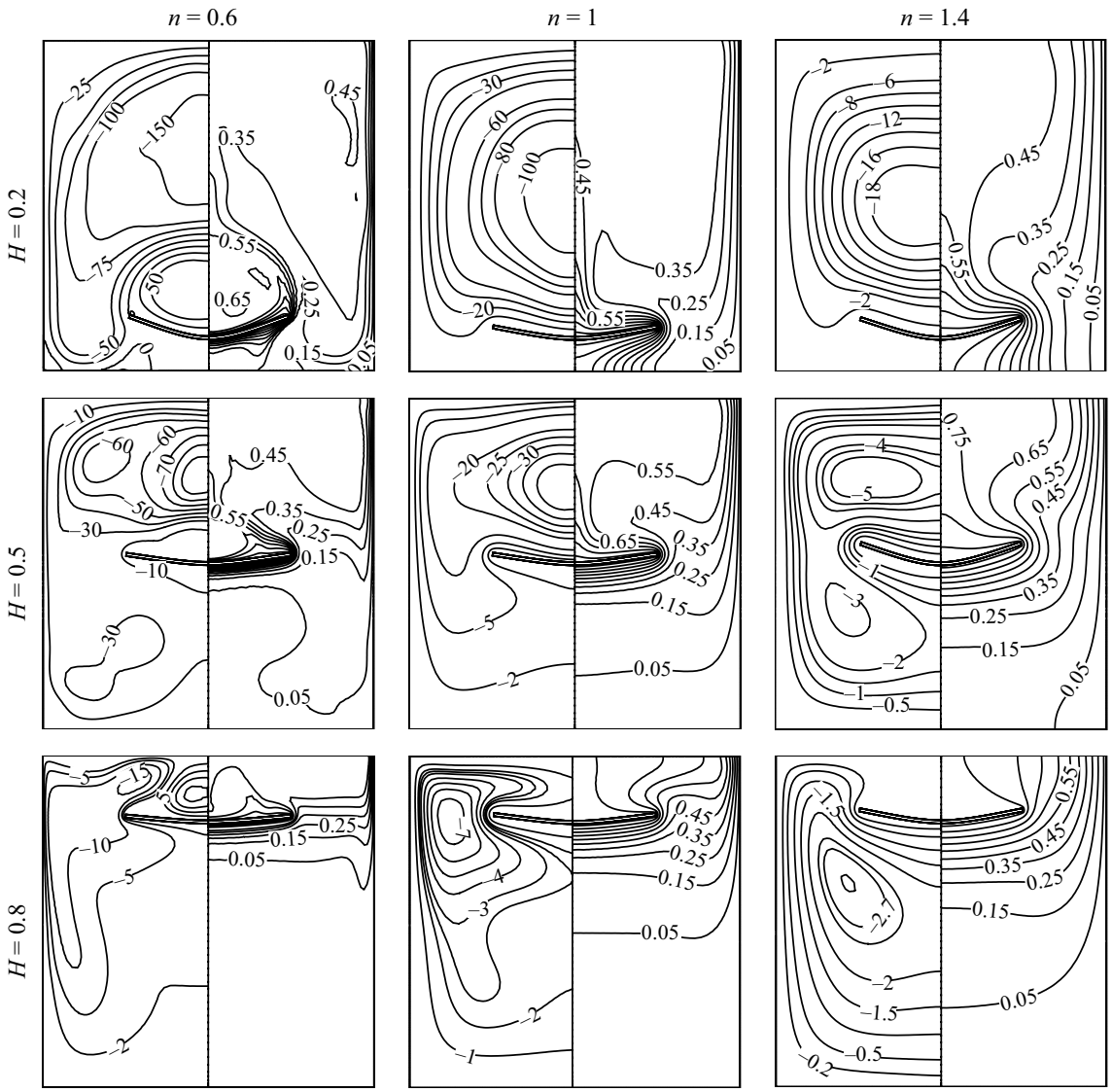

Fig. 10 Effect of the mounting location of the heater (H) on isotherm and streamlines based on $l_p = 0.4$, $\mathrm{Ra} = 10^6$, $\mathrm{Pr} = 10$, $E_\tau = 10^{11}$

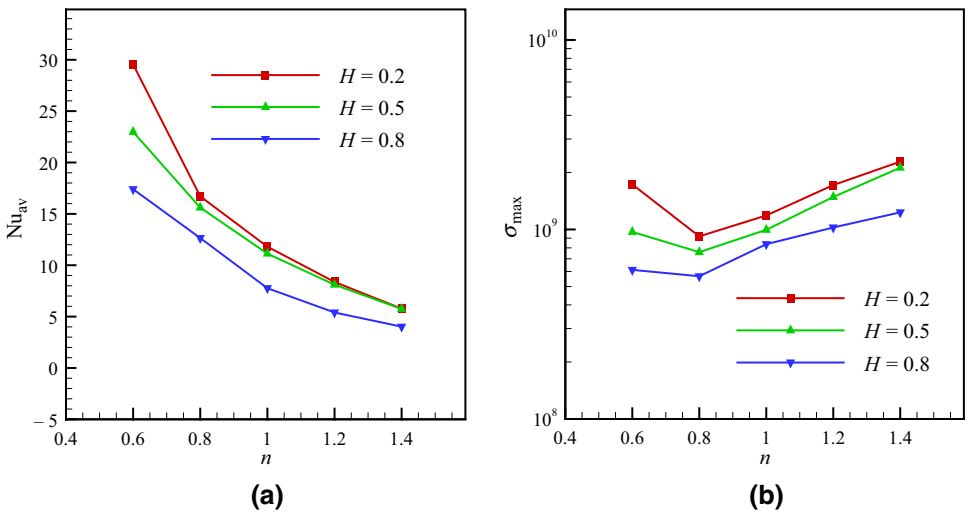

Fig. 11 Variation of **a** the average Nusselt number (Nu_{av}), and **b** the maximum plate stress (σ_{max}) on the plate for select H and a range of n when $l_p = 0.4$, $\mathrm{Pr} = 10$, $E_\tau = 10^{11}$, and $\mathrm{Ra} = 10^6$

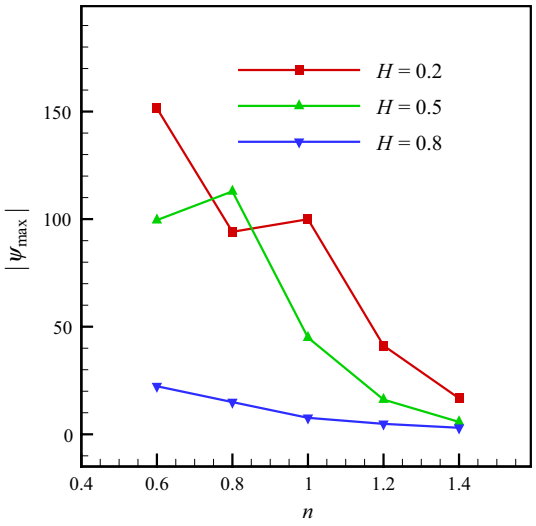

Fig. 12 Variation of maximum streamlines $|\psi_{max}|$ for different power-law index (n) at different mounting locations of the heater (H) when $l_p = 0.4$, $Pr = 10$, $E_\tau = 10^{11}$, and $Ra = 10^6$

stress. As for the effect of n, it can be seen that for low Ra, the stress increases with n while when Ra is increased to 10^6, the stress decreases when n is reduced from 0.6 to 0.8 then starts to increase with n when this latter is further raised until 1.4. This suggests that the stress in the flexible baffle is governed by two mechanisms, the shear stress in the fluid and the strength of the convection, which increases and decreases with n, respectively. For low Ra, the effect of n is more apparent as the intensity of the convection is low. For high Ra, decreasing n for a pseudoplastic fluid decreases the intensity of the flow for relatively similar shear stresses in the fluid. For a dilatant fluid, the intensity of the convective flow declines, and the fluid shear-stresses elevate. The growth of n leads to higher stress in the plate.

Figure 9 illustrates $|\psi_{max}|$ as a function of n for selected Rayleigh numbers. A significant increase of $|\psi_{max}|$ is observed when Ra is increased, mainly for the lower values of n, while this increase is less considerable when n is increased. In fact, the strength of the flow rises when the importance of the viscous forces is diminished compared to the buoyancy forces driving the flow, which is the case for higher Ra. However, the viscous forces are more important when n is increased, which leads to flow with a lower strength compared to lower values of n. The increase in the strength of the flow is equivalent to an increase in the intensity of convection, which is related to the results discussed in Fig. 8.

The effect of the location of the hot plate, i.e., H, on the streamlines and the isotherms is shown in Fig. 10 for selected values of n. It can be seen that for $n = 0.6$, the flow patterns above the plate are similar for all the values of H, but are more or less compressed according to the available size above the plate. Below the plate, the flow is almost not occurring when the plate is too low ($H = 0.2$), while a recirculation zone appears when the plate is in the middle ($H = 0.5$). For $n = 1$ and $n = 1.4$, when the plate is low ($H = 0.2$), the streamlines are concentric curves around the center. When the plate is moved upward, the flow patterns are disturbed around the plate, and an additional vortex appears in the case $n = 1.4$. Concerning the isothermal contours, it is clear that in all the cases, the isothermal contours of low temperature move upward when the hot plate is located in a high position, while naturally, the high-temperature contours are concentrated around the plate.

The variation of Nu_{av} and σ_{max} as functions of n for selected values of H is depicted in Fig. 11. For all the values of n, Nu_{av} increases when H is decreased, i.e., when the hot plate is moved downward. This increase is minimal for higher values of n, as a 35% increase in Nu_{av} is observed when H is reduced from 0.8 to 0.2 for $n = 1.4$, while the value of Nu_{av} is almost doubled for the same reduction of H for $n = 0.6$. This is because of the free convection mechanism, i.e., the hot fluid going upward while the cold fluid is going downward. In fact, moving the hot plate downwards indicates that the fluid is heated in the vicinity of the bottom wall, while the colder fluid is near the top. Moving the hot plate upward reduces the distance between the high- and low-temperature zones and, as a result, reduces the natural convection. For the same reason, the maximum stress is higher when H is decreased for all the values of n, as the convective effects are less developed in that case. It can also be seen that the stress in the plate shows a local minimum at $n = 0.8$ for all the values of H. This is due, as previously explained in Fig. 8, to the fact that the stress over the plate results from two mechanisms, the intensity of convection which vary with H and the shear forces in the fluid which vary with n.

Figure 12 shows $|\psi_{max}|$ as a function of n for selected values of H. When n is equal to or higher than unity (dilatant fluid), $|\psi_{max}|$ decreases when the hot plate is moved upwards. In the case of pseudoplastic fluids, it is shown that for $n = 0.8$, while moving the plate below the middle of the cavity ($H = 0.2$ and $H = 0.5$) increases the value of $|\psi_{max}|$ compared to the case when the plate is above the middle ($H = 0.8$), $|\psi_{max}|$ decreases when H is raised from 0.2 to 0.5. Indeed, the increase in the convective effects due to the reduction of H, as discussed in Fig. 11, leads to a flow with higher strength and a more intense convection.

The impact of the hot plate length, i.e., l_p, on the development of the streamlines and the isotherms for various values of n is illustrated in Fig. 13. First, it can be seen

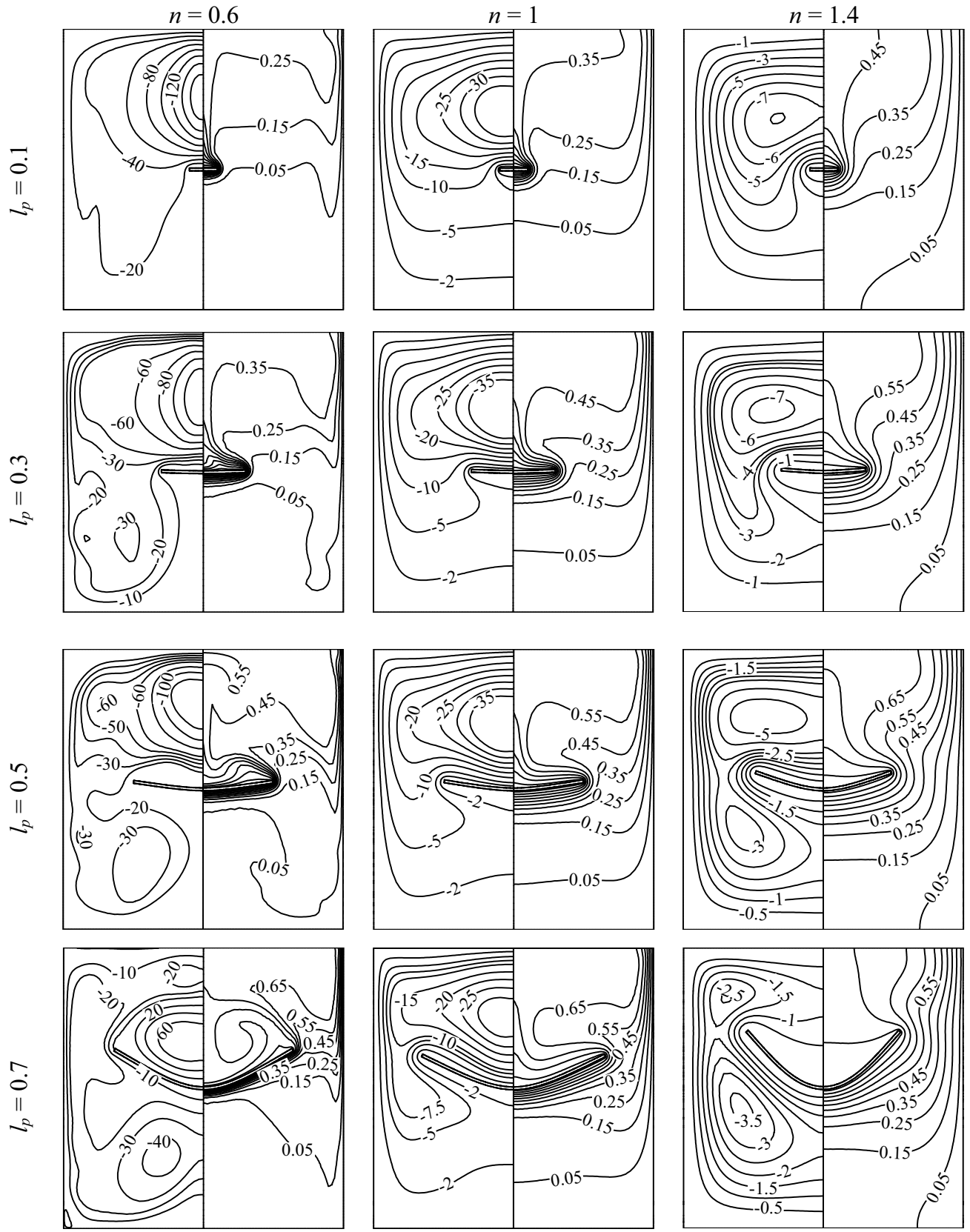

Fig. 13 Effect of the length of the heater (l_p) on isotherm and streamlines based on $H=0.5$, $\mathrm{Ra}=10^6$, $\mathrm{Pr}=10$, $E_\tau=10^{11}$

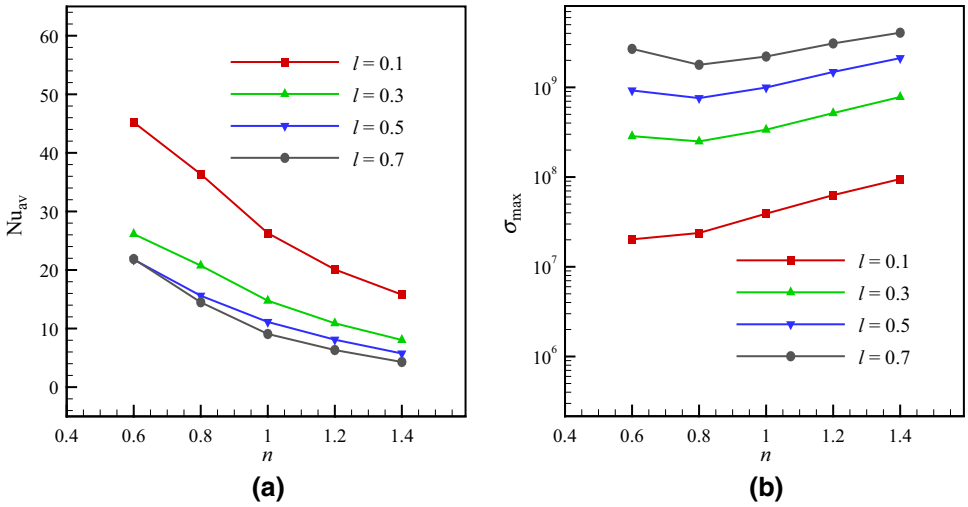

Fig. 14 Behavior of **a** the average Nusselt number (Nu_{av}) and **b** the maximum plate stress (σ_{max}) for a range of n at different l_p at $H=0.5$, $Pr=10$, $E_\tau=10^{11}$, and $Ra=10^6$

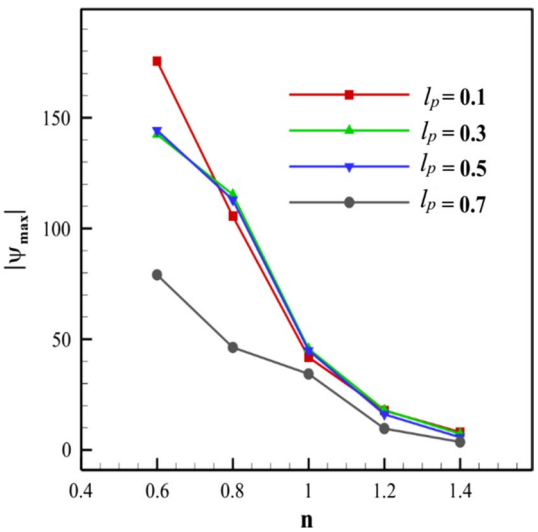

Fig. 15 Variation in the maximum value of the streamlines ($|\psi_{max}|$) at different heater length (l_p) at $H=0.5$, $Pr=10$, $E_\tau=10^{11}$, and $Ra=10^6$

that increasing l_p induces a minimal influence on the flow velocity magnitude. On the other hand, increasing l_p tends to create more disturbance in the flow patterns around the hot plate. In addition, the plate bending is more apparent when it is larger in size. This change of bending can further affect the flow patterns around the plate, like can be seen for instance, by comparing the cases $l_p=0.5$ and $l_p=0.7$ for $n=1.4$. As for the isothermal contours, comparing the same location inside the enclosure for the same value of n but for different values of l_p shows that increasing the size of the plate shows a lower temperature in the location, mainly for temperatures higher than 0.15. This shows that the heat transferred from the plate to the fluid increases with l_p but the comparison with the flow patterns shows that a higher value of l_p reduces the intensity of convection in the cavity.

The profiles of Nu_{av} and σ_{max} are plotted in Fig. 14 for a range of variation of n and selected values of l_p. For all the values of n, Nu_{av} is reduced when l_p increases and is maximum for $l_p=0.1$. Indeed, the presence of a longer plate in the middle of the cavity creates more obstruction to the flow and slows it down which reduces heat transfer by free convection. Nonetheless, as l_p is increased above 0.3, the variation of Nu_{av} becomes less significant. For instance, for $n=0.6$, a 100% increase of Nu_{av} can be noticed when l_p is decreased from 0.7 to 0.1 while Nu_{av} varies slightly when l_p is decreased from 0.7 to 0.5. This indicates that $l_p=0.5$ can be considered as a critical length under which the free convection would be enhanced due to a lower obstruction of the flow. It is worth noting that an increase in the value of Nu_{av} does not indicate an increase in the total heat transfer, as the overall heat transfer is reduced for lower l_p because the surface of heat transfer is decreased. On the other hand, the maximum stress σ_{max} increases when the value of l_p is raised, for the various values of n. This is due to the fact that the contact area of the fluid–structure interaction is increased, and, thus, the interaction forces acting upon it are enhanced.

Figure 15 depicts the variation of $|\psi_{max}|$ as a function of n for different values of l_p. For $n>0.8$, the value of $|\psi_{max}|$ shows very little variation when l_p is below 0.5. for $n=0.6$, $|\psi_{max}|$ increases substantially to a maximum value when $l_p=0.1$ compared to the other cases. For all the values of n, $|\psi_{max}|$ is always minimum for $l_p=0.7$. As indicated previously, increasing the length if the plate obstructs the flow and reduces its strength as well as the intensity of convection.

Conclusions

In the current work, the flow and heat transfer of pseudoplastic and dilatant liquids were investigated in a cavity containing a thin hot plate. The large displacements of the plate due to the fluid interaction were modeled by the ALE approach. The governing equations for the displacement of the plate and the flow and heat transfer in the liquid were introduced in the form of partial differential equations and transformed into a non-dimensional form. The PDE equations were written in a weak form and solved by FEM. The effect of mesh size on the accuracy of the results was investigated. The simulation outcomes for some marginal cases were compared with the literature results and found in good agreement. The influence of the important non-dimensional parameters on the streamlines, isotherms, and Nusselt number was addressed. The main outcomes of the present numerical analysis can be summarized as follows:

- Increasing the power-law index of the non-Newtonian fluid, i.e., n, raises the apparent viscosity and reduces the strength of the flow and the intensity of convection. The heat transfer is thus more enhanced in the case of a pseudoplastic (shear-thinning) fluid compared to a dilatant (shear-thickening) fluid. On the other hand, increasing n leads to higher stress over the flexible plate due to a higher magnitude of the fluid–structure interaction force.
- Using a higher value of Rayleigh number, i.e., Ra, increases the relative importance of the buoyancy forces driving the flow compared to the viscous forces and leads to higher convection intensity. Consequently, the heat transfer by natural convection is enhanced. This enhancement is less important for high values of n where the viscous effects remain more pronounced. Increasing Ra from 10^4 to 10^6 raises the value of Nu_{av} by 3.5 times for $n=0.6$ and by 1.5 times for $n=1.4$.
- Raising the position of the hot plate inside the enclosure reduces the vertical distance between the hot and cold zones in the fluid and, as a result, diminishes the intensity of convection and the resulting heat transfer. This is valid for all the values of n. Nu_{av} increases by 35% when H is decreased from 0.8 to 0.2 for $n=1.4$, while Nu_{av} is doubled for the same decrease of H when $n=0.6$.
- Using a longer flexible plate leads to a more obstruction of the flow, which decreases the intensity of convection. Increasing the length of the plate l_p thus weakens the average heat transfer by free convection. Nu_{av} is almost doubled when l_p is reduced from 0.7 to 0.1 while Nu_{av} changes slightly when l_p is reduced from 0.7 to 0.5. Nonetheless, due to the increased size of the plate, the stress acting over it rises.

References

1. Alsabery A, Yazdi M, Altawallbeh A, Hashim I. Effects of non-homogeneous nanofluid model on convective heat transfer in partially heated square cavity with conducting solid block. J Therm Anal Calorim. 2019;136(4):1489–514.
2. Alsabery A, Armaghani T, Chamkha A, Hashim I. Conjugate heat transfer of Al_2O_3–water nanofluid in a square cavity heated by a triangular thick wall using Buongiorno's two-phase model. J Therm Anal Calorim. 2019;135(1):161–76.
3. Benkhedda M, Boufendi T, Tayebi T, Chamkha AJ. Convective heat transfer performance of hybrid nanofluid in a horizontal pipe considering nanoparticles shapes effect. J Therm Anal Calorim. 2020;140(1):411–25.
4. Tayebi T, Chamkha AJ. Entropy generation analysis due to MHD natural convection flow in a cavity occupied with hybrid nanofluid and equipped with a conducting hollow cylinder. J Therm Anal Calorim. 2020;139(3):2165–79.
5. Dogonchi A, Nayak M, Karimi N, Chamkha AJ, Ganji D. Numerical simulation of hydrothermal features of Cu–H_2O nanofluid natural convection within a porous annulus considering diverse configurations of heater. J Therm Anal Calorim. 2020. https://doi.org/10.1007/s10973-020-09419-y.
6. Al-Amiri A, Khanafer K. Fluid–structure interaction analysis of mixed convection heat transfer in a lid-driven cavity with a flexible bottom wall. Int J Heat Mass Transf. 2011;54(17–18):3826–36.
7. Khanafer K. Fluid–structure interaction analysis of non-Darcian effects on natural convection in a porous enclosure. Int J Heat Mass Transf. 2013;58(1–2):382–94.
8. Khanafer K. Comparison of flow and heat transfer characteristics in a lid-driven cavity between flexible and modified geometry of a heated bottom wall. Int J Heat Mass Transf. 2014;78:1032–41.
9. Soti AK, Bhardwaj R, Sheridan J. Flow-induced deformation of a flexible thin structure as manifestation of heat transfer enhancement. Int J Heat Mass Transf. 2015;84:1070–81.
10. Joshi RU, Soti AK, Bhardwaj R. Numerical study of heat transfer enhancement by deformable twin plates in laminar heated channel flow. Comput Therm Sci Int J. 2015;7(5–6):1–10.
11. Ali S, Habchi C, Menanteau S, Lemenand T, Harion J-L. Heat transfer and mixing enhancement by free elastic flaps oscillation. Int J Heat Mass Transf. 2015;85:250–64.
12. Han D, Liu G, Abdallah S. An Eulerian–Lagrangian–Lagrangian method for 2D fluid–structure interaction problem with a thin flexible structure immersed in fluids. Comput Struct. 2020;228:106179.
13. Han D, Liu G, Abdallah S. An Eulerian–Lagrangian–Lagrangian method for solving fluid–structure interaction problems with bulk solids. J Comput Phys. 2020;405:109164.
14. Truong H, Engels T, Kolomenskiy D, Schneider K. A mass-spring fluid–structure interaction solver: application to flexible revolving wings. Comput Fluids. 2020;200:104426.
15. Selimefendigil F, Öztop HF, Abu-Hamdeh N. Mixed convection due to rotating cylinder in an internally heated and flexible walled cavity filled with SiO_2–water nanofluids: effect of nanoparticle shape. Int Commun Heat Mass Transf. 2016;71:9–19.
16. Selimefendigil F, Öztop HF. Mixed convection in a two-sided elastic walled and SiO_2 nanofluid filled cavity with internal heat generation: effects of inner rotating cylinder and nanoparticle's shape. J Mol Liq. 2015;212:509–16.
17. Selimefendigil F, Öztop HF. Analysis of MHD mixed convection in a flexible walled and nanofluids filled lid-driven cavity with volumetric heat generation. Int J Mech Sci. 2016;118:113–24.

18. Alsabery A, Selimefendigil F, Hashim I, Chamkha A, Ghalambaz M. Fluid–structure interaction analysis of entropy generation and mixed convection inside a cavity with flexible right wall and heated rotating cylinder. Int J Heat Mass Transf. 2019;140:331–45.
19. Alsabery A, Mohebbi R, Chamkha A, Hashim I. Impacts of magnetic field and non-homogeneous nanofluid model on convective heat transfer and entropy generation in a cavity with heated trapezoidal body. J Therm Anal Calorim. 2019;138(2):1371–94.
20. Selimefendigil F, Öztop HF. Mixed convection in a partially heated triangular cavity filled with nanofluid having a partially flexible wall and internal heat generation. J Taiwan Inst Chem Eng. 2017;70:168–78.
21. Selimefendigil F, Öztop HF, Chamkha AJ. Fluid–structure–magnetic field interaction in a nanofluid filled lid-driven cavity with flexible side wall. Eur J Mech B/Fluids. 2017;61:77–85.
22. Selimefendigil F, Öztop HF, Chamkha AJ. Analysis of mixed convection of nanofluid in a 3D lid-driven trapezoidal cavity with flexible side surfaces and inner cylinder. Int Commun Heat Mass Transf. 2017;87:40–51.
23. Jamesahar E, Ghalambaz M, Chamkha AJ. Fluid–solid interaction in natural convection heat transfer in a square cavity with a perfectly thermal-conductive flexible diagonal partition. Int J Heat Mass Transf. 2016;100:303–19.
24. Mehryan S, Ghalambaz M, Ismael MA, Chamkha AJ. Analysis of fluid–solid interaction in MHD natural convection in a square cavity equally partitioned by a vertical flexible membrane. J Magn Magn Mater. 2017;424:161–73.
25. Mehryan S, Chamkha A, Ismael M, Ghalambaz M. Fluid–structure interaction analysis of free convection in an inclined square cavity partitioned by a flexible impermeable membrane with sinusoidal temperature heating. Meccanica. 2017;52(11–12):2685–703.
26. Alshuraiaan B, Khanafer K. The effect of the position of the heated thin porous fin on the laminar natural convection heat transfer in a differentially heated cavity. Int Commun Heat Mass Transf. 2016;78:190–9.
27. Ali S, Menanteau S, Habchi C, Lemenand T, Harion J-L. Heat transfer and mixing enhancement by using multiple freely oscillating flexible vortex generators. Appl Therm Eng. 2016;105:276–89.
28. Ghalambaz M, Jamesahar E, Ismael MA, Chamkha AJ. Fluid–structure interaction study of natural convection heat transfer over a flexible oscillating fin in a square cavity. Int J Therm Sci. 2017;111:256–73.
29. Ismael MA, Jasim HF. Role of the fluid–structure interaction in mixed convection in a vented cavity. Int J Mech Sci. 2018;135:190–202.
30. Alsabery A, Sheremet M, Ghalambaz M, Chamkha A, Hashim I. Fluid–structure interaction in natural convection heat transfer in an oblique cavity with a flexible oscillating fin and partial heating. Appl Therm Eng. 2018;145:80–97.
31. Selimefendigil F, Oztop HF, Chamkha AJ. MHD mixed convection in a nanofluid filled vertical lid-driven cavity having a flexible fin attached to its upper wall. J Therm Anal Calorim. 2019;135(1):325–40.
32. Yaseen DT, Ismael MA. Analysis of power law fluid–structure interaction in an open trapezoidal cavity. Int J Mech Sci. 2020;174:105481.
33. Sabbar WA, Ismael MA, Almudhaffar M. Fluid–structure interaction of mixed convection in a cavity-channel assembly of flexible wall. Int J Mech Sci. 2018;149:73–83.
34. Sun X, Ye Z, Li J, Wen K, Tian H. Forced convection heat transfer from a circular cylinder with a flexible fin. Int J Heat Mass Transf. 2019;128:319–34.
35. Selimefendigil F, Öztop HF. Fluid–solid interaction of elastic-step type corrugation effects on the mixed convection of nanofluid in a vented cavity with magnetic field. Int J Mech Sci. 2019;152:185–97.
36. Saleh H, Siri Z, Hashim I. Role of fluid–structure interaction in mixed convection from a circular cylinder in a square enclosure with double flexible oscillating fins. Int J Mech Sci. 2019;161:105080.
37. Raisi A, Arvin I. A numerical study of the effect of fluid–structure interaction on transient natural convection in an air-filled square cavity. Int J Therm Sci. 2018;128:1–14.
38. Zadeh SMH, Mehryan S, Izadpanahi E, Ghalambaz M. Impacts of the flexibility of a thin heater plate on the natural convection heat transfer. Int J Therm Sci. 2019;145:106001.
39. Mehryan S, Alsabery A, Modir A, Izadpanahi E, Ghalambaz M. Fluid–structure interaction of a hot flexible thin plate inside an enclosure. Int J Therm Sci. 2020;153:106340.
40. Ghalambaz M, Mehryan S, Alsabery AI, Hajjar A, Izadi M, Chamkha A. Controlling the natural convection flow through a flexible baffle in an L-shaped enclosure. Meccanica. 2020. https://doi.org/10.1007/s11012-020-01194-2.
41. Mehryan SAM, Izadpanahi E, Ghalambaz M, Chamkha AJ. Mixed convection flow caused by an oscillating cylinder in a square cavity filled with Cu–Al_2O_3/water hybrid nanofluid. J Therm Anal Calorim. 2019. https://doi.org/10.1007/s10973-019-08012-2.
42. The Finite Element Method for Fluid Dynamics. In: Zienkiewicz OC, Taylor RL, Nithiarasu P, editors. The finite element method for fluid dynamics (Seventh Edition). Oxford: Butterworth-Heinemann; 2014. p. iii.
43. Küttler U, Wall WA. Fixed-point fluid–structure interaction solvers with dynamic relaxation. Comput Mech. 2008;43(1):61–72.
44. Matin MH, Khan WA. Laminar natural convection of non-Newtonian power-law fluids between concentric circular cylinders. Int Commun Heat Mass Transf. 2013;43:112–21.
45. Saravanan S, Sivaraj C. Combined natural convection and thermal radiation in a square cavity with a nonuniformly heated plate. Comput Fluids. 2015;117:125–38. https://doi.org/10.1016/j.compfluid.2015.05.005.